Scaled Silicon MOSFET's: Degradation of the Total Gate Capacitance

Dragica Vasileska, Dieter K. Schroder, *Fellow, IEEE*, and David K. Ferry, *Fellow, IEEE*

***Abstract*— We use a fully quantum-mechanical model to study the influence of image and exchange-correlation effects on the inversion layer and total gate capacitance in scaled Si MOSFET's. We show that, when the device is in weak and moderate inversion, the inclusion of image and many-body exchange-correlation effects increases both the inversion layer and total gate capacitances and shifts the $N_s = N_s(V_G)$ characteristics of the device toward lower gate voltages.**

I. Introduction

As MOSFET's scale to shorter channel lengths, channel doping densities increase in order to supress undesirable short-channel effects such as punchthrough and drain-induced barrier lowering. The quasi-two-dimensional (Q-2-D) nature of the carrier transport in these state-of-the-art devices due to heavy substrate doping affects several measurable quantities, such as effective electron and hole mobilities, inversion charge density, threshold voltage, and total gate capacitance ($C_{\rm tot}$). The latter determines the magnitude of the transconductance.

During the last few years, a significant amount of research has been done to estimate the degradation of the total gate capacitance in devices with very thin gate oxides. The inversion layer capacitance ($C_{\rm inv}$) [1] has been experimentally characterized and identified as the main cause of a second-order thickness dependence in the MOSFET characteristics [2]–[6]. Recent theoretical calculations by Hareland *et al.* [7] confirmed these experimental findings. These authors demonstrated that the finite inversion layer capacitance leads to significant degradation of the total gate capacitance in deep submicron devices. However, in their calculations they used the Fang–Howard [8] variational wavefunction for the ground subband and calculated the energies of the higher lying subbands by using a perturbation technique due to Stern [9]. In addition, in order to obtain better overall agreement with the self-consistent results from [9], they introduced a correction factor of -10 mV to the variationally calculated eigenenergies for which they do not give any physical explanation.

The two physical origins of the inversion layer capacitance, a classical one due to the finite density of states, and a quantum-mechanical one due to the finite inversion layer thickness and movement of the charge away from the surface, have also been identified experimentally [6] as well as theoretically [7]. However, nobody has yet studied the influence of image and many-body exchange-correlation effects on the magnitude of the inversion layer and total gate capacitance, a point upon which we focus in this paper.

Manuscript received April 19, 1996; revised September 4, 1996. The review of this paper was arranged by Editor J. R. Hauser. This work was supported by the Office of Naval Research.

The authors are with the Center for Solid State Electronics Research, Arizona State University, Tempe, AZ 85287-6206 USA.

Publisher Item Identifier S 0018-9383(97)02234-X.

II. Calculation of the Subband Structure

To describe the system more realistically such that the results obtained can reflect the experimental situation, we calculate the envelope wavefunctions and the corresponding bound-state energies in the direction perpendicular to the interface (z-axis) by solving self-consistently the one-dimensional (1-D) Poisson and Schrödinger equations, with the latter expressed in the form given by Hohenberg and Kohn [10], and Kohn and Sham [11]. The one-particle Hohenberg–Kohn–Sham (HKS) equation has an effective potential energy term which consists of the sum of the Hartree, image, and exchange-correlation terms.[1] The Hartree potential, due to the electrostatic interaction of the electrons with themselves and with ionized impurities, is determined from the numerical solution of the Poisson equation. For the evaluation of the image term, which arises because of the different dielectric constants of the semiconductor and oxide, we use the conventional result given in [12], [13]. We approximate the exchange-correlation potential energy term by an interpolation formula developed by Hedin and Lundqvist [14], which is accurate over a large density range. We want to emphasize that, although the numerical calculation of the subband structure becomes much more computationally involved, it gives us the freedom to study devices with arbitrary doping profiles.

In all calculations presented here, we assume that the p-Si/SiO_2 interface is parallel to a [100] plane. For this orientation of the interface, the six equivalent minima of the bulk silicon conduction band (located 85% away from the Γ point toward the X point of the first Brillouin zone) split into two sets of subbands. One set consists of the two equivalent valleys which have the longitudinal mass perpendicular to the interface ($m_z = m_l = 0.91 m_o$ and $m_{xy} = m_t = 0.19 m_o$). Following the notation of Stern [15], the energy levels associated with this set of equivalent

[1] According to the density functional theory of Hohenberg and Kohn [10], and Kohn and Sham [11], the effects of exchange and correlation can be included through a one-particle exchange-correlation term $V_{\rm xc}[n(z)]$ defined as the functional derivative of the exchange-correlation part of the ground-state energy $E_{\rm xc}$ with respect to electron density $n(z)$. In the local density approximation, $E_{\rm xc}$ is approximated by the product of the local electron density and the exchange-correlation energy per electron of a uniform electron gas with density $n = n(z)$. Thus, $V_{\rm xc}[n(z)]$ can be interpreted as equivalent to the exchange-correlation part of the Fermi energy for a uniform system.

0018–9383/97$10.00 © 1997 IEEE

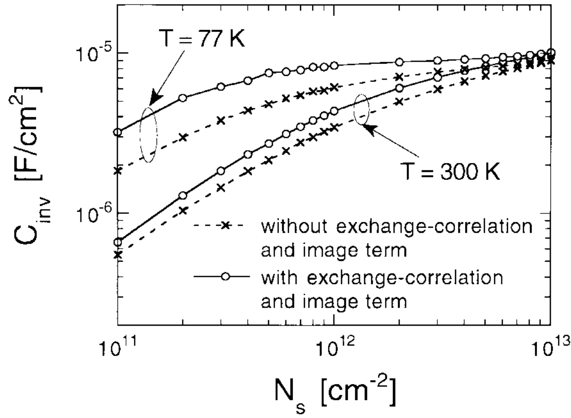

Fig. 1. Variation of the inversion layer capacitance with inversion charge density. Solid (dashed) lines represent the case when image and many-body exchange-correlation effects are included (omitted) in the calculation of the subband structure.

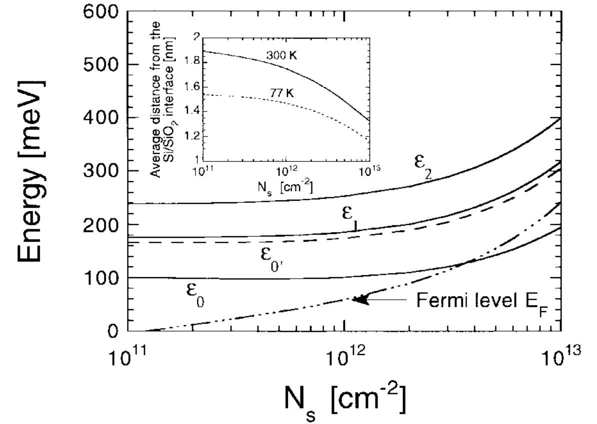

Fig. 2. Variation of the energies of the lowest four subbands and the position of the Fermi level with inversion charge density for the device from Fig. 1 at $T = 300$ K. All energies are measured from the bottom of the conduction band at the Si/SiO$_2$ interface. In the inset we show the variation of the centroid of the electron density distribution with inversion charge density at $T = 77$ K and $T = 300$ K.

valleys are $\varepsilon_0, \varepsilon_1, \varepsilon_2, \ldots$, where ε_0 is the energy of the ground subband. The energy levels for the other four equivalent valleys, with the light mass in the direction perpendicular to the interface $(m_z = m_t = 0.19m_o$ and $m_{xy} = \sqrt{m_l m_t} = 0.42m_o)$ are $\varepsilon_0', \varepsilon_1', \varepsilon_2', \ldots$. Thus, to find the energy levels associated with these two subband ladders, at each iteration step we solve the HKS equation twice. More numerical details of our code can be found in [16] and [17].

III. Simulation Results for $C_{\rm inv}$ and $C_{\rm tot}$

The total gate capacitance, which determines the MOSFET's transconductance as well as the magnitude of the inversion charge density in the channel, is defined as

$$C_{\rm tot} = \frac{dQ_G}{dV_G}. \quad (1)$$

In (1), dQ_G is the change of the gate charge due to a dV_G gate voltage change. From the charge-neutrality condition in the device it follows that $Q_G = -Q_{\rm sc} = e(N_s + N_{\rm depl})$. Since the total gate voltage equals the sum of the voltage drop across the oxide $(V_{\rm ox})$ and the voltage drop across the semiconductor $(V_{\rm sc})$, (1) can be rewritten as [18]

$$C_{\rm tot} = \frac{C_{\rm ox}}{1 + C_{\rm ox}/(C_{\rm inv} + C_{\rm depl})}. \quad (2)$$

Here, $C_{\rm ox} = dQ_G/dV_{\rm ox}$ is the oxide capacitance and $C_{\rm depl} = qdN_{\rm depl}/dV_{\rm sc}$ is the depletion layer capacitance.[2] Since $C_{\rm depl}$ is much smaller in magnitude than $C_{\rm inv}$, its contribution to the total gate capacitance can safely be ignored. In deriving the result given in (2), we have assumed that there are no interface-traps at the Si/SiO$_2$ interface.

Equation (2) suggests that devices with thick gate oxides (several hundred angstroms thick) have total gate capacitance approximately equal to the oxide capacitance. The situation changes for MOSFET's with very thin gate oxides (less than 10 nm thick). In these devices, the oxide capacitance is comparable in magnitude to $C_{\rm inv}$ which, as follows from (2), makes the total gate capacitance significantly lower than the oxide capacitance. Since the device scaling rules demand thinner gate oxides, the degradation of the total gate capacitance, which defines MOSFET's transconductance, is expected to have very important consequences on their performance.

To justify the above arguments quantitatively and estimate the degree of degradation of the total gate capacitance in future submicron devices, first, in Fig. 1, we show the variation of the inversion layer capacitance with inversion charge density for a device with $N_a = 7\times10^{17}$ cm^{-3}. We want to point out that, in contrast to some previous studies [1], [2], [5] where $C_{\rm inv}$ was approximated with $\varepsilon_{\rm sc}/\langle z\rangle_{\rm av}$ [$\langle z\rangle_{\rm av}$ is the average inversion-layer thickness], in this work we employ the general definition for $C_{\rm inv} = qdN_s/dV_{\rm sc}$ and make use of the self-consistent results for N_s and $V_{\rm sc}$.

We find that at $T = 77$ K and $T = 300$ K, the inversion layer capacitance increases with increasing N_s. We also observe that $C_{\rm inv}$ has a smaller N_s dependence at high values of N_s. The inclusion of image and many-body exchange-correlation effects is found to increase $C_{\rm inv}$, and this increase is quite large at low values of N_s. For example, for $N_s = 10^{11}$ cm^{-2} and $T = 300$ K ($T = 77$ K), simulation results for $C_{\rm inv}$ are higher by approximately 20% (74%) when these two effects are included in the calculation of the subband structure. However, their influence is found to decrease proportionally with increasing N_s (the exchange-correlation contribution to the inversion layer capacitance is relatively constant as N_s is varied). The observed slope change in the $C_{\rm inv}$ versus N_s data comes from the fact that the total inversion layer capacitance can be described as a series capacitance of the following two contributions:

$$\begin{aligned}\frac{1}{C_{\rm inv}} &= \frac{1}{\sum_n \rho_n\left[1+\exp\left(\frac{\varepsilon_n - E_F}{k_BT}\right)\right]^{-1}} \\ &\quad + \frac{e^2}{2\varepsilon_{\rm sc}} \frac{\sum_n \rho_n \langle z\rangle_n \left[1+\exp\left(\frac{\varepsilon_n - E_F}{k_BT}\right)\right]^{-1}}{\sum_n \rho_n\left[1+\exp\left(\frac{\varepsilon_n - E_F}{k_BT}\right)\right]^{-1}} \\ &= \frac{1}{\sum_n \rho_n[1-\exp(-N_n/k_BT\rho_n)]} \\ &\quad + \frac{e^2}{2\varepsilon_{\rm sc}} \frac{\sum_n \rho_n\langle z\rangle_n[1-\exp(-N_n/k_BT\rho_n)]}{\sum_n \rho_n[1-\exp(-N_n/k_BT\rho_n)]}. \end{aligned} \quad (3)$$

[2] Since we have defined the charge in (1) as charge per unit area, all capacitance that appear in (2) are capacitances per unit area.

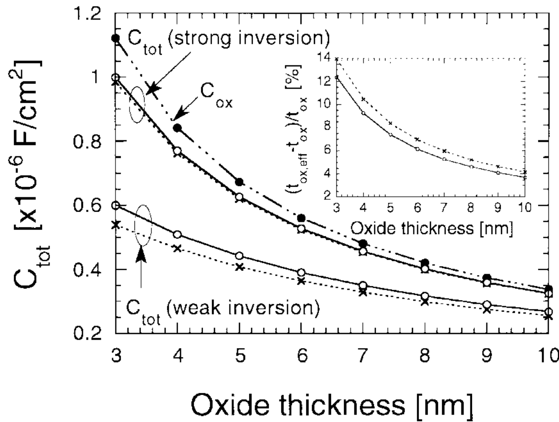

Fig. 3. Variation of the total gate capacitance with oxide thickness at $T = 300$ K when the device from Fig. 1 is driven into the weak ($N_s = 2 \times 10^{11}$ cm^{-2}) and strong ($N_s = 7 \times 10^{12}$ cm^{-2}) inversion regime. In the inset we show the relative error between the experimentally derived oxide thickness and the physical oxide thickness of the device when in strong inversion. Solid (dashed) lines correspond to the case when image and many-body exchange-correlation effects are included (omitted) in the calculation of the subband structure.

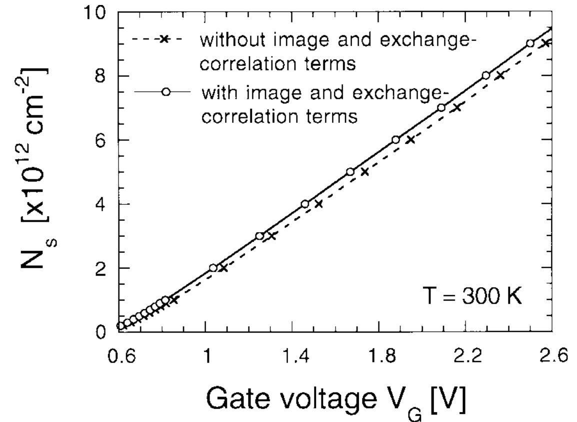

Fig. 4. Inversion charge density versus gate voltage for the device with 4-nm gate oxide thickness. Solid (dashed) lines correspond to the case when image and many-body exchange-correlation effects are included (omitted) in the solution of the eigenvalue problem.

Here, ρ_n is the two-dimensional (2-D) density of states function of the n-th subband from either the unprimed or primed ladder of subbands, E_F is the Fermi energy, k_B is the Boltzmann constant, T is the temperature and $\langle z \rangle_n$ is the average distance of the inversion layer electrons residing in the n-th subband from the interface.[3] The first contribution to $C_{\rm inv}$ [first term in (3)] is the classical one due to the finite density of states and dominates at low gate voltages ($N_s < 2 \times 10^{12}$ cm^{-2}). As shown in Fig. 2, where we plot the Fermi energy as well as the subband energies, this contribution to $C_{\rm inv}$ comes from the fact that, as the inversion charge density increases, the Fermi level moves upward. In this region, the shape of the confining potential is dictated by the very high doping concentration ($N_{\rm depl} \approx 3 \times 10^{12}$ cm^{-2}) so that the energies of the bound states in the well are nearly constant. The second contribution to $C_{\rm inv}$ is due to the finite quantum-mechanical inversion layer thickness [second term in expression (3)], and dominates at high gate voltages, i.e., for $N_s > 2 \times 10^{12}$ cm^{-2}. In this region, due to a significant inversion charge contribution to the band-bending and the steeper rise of the conduction band near the Si/SiO_2 interface, the bound state energies increase with increasing N_s. The opposite is true for $\langle z \rangle_n$; it decreases with increasing N_s due to the reduction of the width of the well. At high enough values of N_s, the increase of the term $[1 - \exp(-N_n/k_B T \rho_n)]$ and the decrease of $\langle z \rangle_{\rm av} = \sum_n N_n \langle z \rangle_n / N_s$ (see the inset of Fig. 2) nearly cancel each other which gives the inversion layer capacitance $C_{\rm inv}$ a weaker dependence on N_s.

The influence of the inversion layer capacitance on the total gate capacitance is shown in Fig. 3. We find that the degradation of $C_{\rm tot}$ increases with decreasing gate oxide thickness $t_{\rm ox}$. For example, for a device with $t_{\rm ox} = 3$ nm and $N_s = 2 \times 10^{11}$ cm^{-2} ($N_s = 7 \times 10^{12}$ cm^{-2}), the degradation of the total gate capacitance is $(C_{\rm ox} - C_{\rm tot})/C_{\rm ox} = 46.5\%$ (11%). We also find that in weak inversion, where the degradation of $C_{\rm tot}$ is the largest, the inclusion of the image and many-body exchange-correlation effects improves the situation. As previously, their influence decreases with increasing N_s. Since smaller gate capacitance means smaller carrier density in the channel, the results shown in this figure suggest that the degradation of $C_{\rm tot}$ will impose crucial limitations on the lower voltage operation of future submicron devices.

The relative error between the electrically inferred effective oxide thickness from the capacitance–voltage (C–V) measurements ($t_{\rm ox,eff} = \varepsilon_{\rm ox}/C_{\rm tot}$) and the physical oxide thickness ($t_{\rm ox} = \varepsilon_{\rm ox}/C_{\rm ox}$) is shown in the inset of Fig. 3. Since quantum-mechanically calculated charge distribution is always peaked at some finite distance from the interface (see the inset of Fig. 2), the effective oxide thickness inferred from the C–V measurements is always larger than the physical oxide thickness. The discrepancy between the two increases with decreasing $t_{\rm ox}$. We also calculate that, even though image and many-body exchange-correlation effects do not significantly affect the magnitude of the total gate capacitance in strong inversion, the inclusion of these two effects leads to a reduction of the relative error between the electrically inferred and the physical oxide thickness by about 2% in devices with ultra-thin gate oxides ($t_{\rm ox} < 4$ nm).

The room-temperature $N_s = N_s(V_G)$ characteristics of the device with substrate doping density $N_a = 7 \times 10^{17}$ cm^{-3} and 4-nm gate oxide thickness are shown in Fig. 4. As expected, the inversion charge density varies linearly with the gate voltage except in the subthreshold region. The $N_s = N_s(V_G)$ characteristics shift toward lower gate voltages when image and exchange-correlation terms are accounted for in the calculation of the subband structure. In strong inversion (large gate voltages), the voltage shift is calculated to be of the order of 70 mV.

IV. CONCLUSION

We have demonstrated that image and exchange-correlation effects increase the inversion layer capacitance when the device is in weak and moderate inversion, which leads to

[3] This expression is a finite temperature generalization of the zero-temperature result calculated by Frank Stern that is given in [5].

higher total gate capacitance. Their influence is found to be insignificant in strong inversion. We also showed that the degradation of the total gate capacitance due to finite inversion layer capacitance is significant in scaled silicon MOSFET's. Since the key factor that leads to reduced short-channel effects is the amount of gate control on the channel charge [19], the results presented in Fig. 4 imply that the omission of the image and exchange-correlation effects in the subband structure calculations can affect the predicted device performance.

Acknowledgment

The authors would like to thank C. Ringhofer, Arizona State University, P. Bordone, Universitá di Modena, and T. Eldridge, McDonnell Douglas Helicopter Systems, for valuable discussions.

References

[1] S. Luryi, "Quantum capacitance devices," *Appl. Phys. Lett.*, vol. 52, pp. 501–503, 1988.
[2] G. Baccarani and M. R. Wordeman, "Transconductance degradation in thin-oxide MOSFET's," in *IEDM Tech. Dig.*, 1982, pp. 278–281.
[3] S.-Y. Oh, S.-G. Choi, C. G. Sodini, and J. L. Moll, "Analysis of the channel inversion layer capacitance in very thin gate IGFET," *IEEE Electron Device Lett.*, vol. EDL-4, pp. 236–239, 1983.
[4] M.-S. Liang, J. Y. Choi, P.-K. Ko, and C. Hu, "Inversion-layer capacitance and mobility of very thin gate oxide MOSFET's," *IEEE Trans. Electron Devices*, vol. ED-33, pp. 409–413, 1986.
[5] A. Hartstein and N. F. Albert, "Determination of the inversion-layer thickness from capacitance measurements of metal-oxide-semiconductor field-effect transistors with ultrathin oxide layers," *Phys. Rev. B*, vol. 38, pp. 1235–1240, 1988.
[6] S. Takagi and A. Toriumi, "Quantitative understanding of inversion-layer capacitance in Si MOSFET's," *IEEE Trans. Electron Devices*, vol. 42, pp. 2125–2130, 1995.
[7] S. A. Hareland, S. Krishnamurthy, S. Jallepalli, C.-F. Yeap, K. Hasnat, A. F. Tasch, Jr., and C. M. Maziar, "A computationally efficient model for inversion layer quantization effects in deep submicron N-channel MOSFET's," *IEEE Trans. Electron Devices*, vol. 43, pp. 90–96, 1996.
[8] F. F. Fang and W. E. Howard, "Negative field-effect mobility on (100) Si surfaces," *Phys. Rev. Lett.*, vol. 16, pp. 797–799, 1966.
[9] F. Stern, "Self-consistent results for n-type Si inversion layers," *Phys. Rev. B*, vol. 5, pp. 4891–4899, 1972.
[10] P. Hohenberg and W. Kohn, "Inhomogeneous electron gas," *Phys. Rev.*, vol. 136, pp. B864–B871, 1964.
[11] W. Kohn and L. J. Sham, "Self-consistent equations including exchange and correlation effects," *Phys. Rev.*, vol. 140, pp. A1133–A1140, 1965.
[12] F. Stern, "Image potential near a gradual interface between two dielectrics," *Phys. Rev. B*, vol. 17, pp. 5009–5015, 1978.
[13] J. D. Jackson, *Classical Electrodynamics*. New York: Wiley, 1975.
[14] L. Hedin and B. I. Lundqvist, "Explicit local exchange-correlation potentials," *J. Phys. C: Solid State Phys.*, vol. 4, pp. 2064–2083, 1971.
[15] F. Stern, "Iteration methods for calculating self-consistent fields in semiconductor inversion layers," *J. Comp. Phys.*, vol. 6, pp. 56–67, 1970.
[16] D. Vasileska, P. Bordone, T. Eldridge, and D. K. Ferry, "Quantum transport simulation of the DOS function, self-consistent fields and mobility in MOS inversion layers," to be published.
[17] D. Vasileska, "Green's functions formalism for low-dimensional systems," Ph.D. dissertation, Arizona State Univ., Tempe, Dec. 1995.
[18] D. K. Schroder, *Semiconductor Material and Device Characterization*. New York: Wiley, 1990.
[19] B. Agrawal, V. K. De, and J. D. Meindl, "Device parameter optimization for reduced short channel effects in retrograde doping MOSFET's," *IEEE Trans. Electron Devices*, vol. 43, pp. 365–368, 1996.

Dragica Vasileska, for a photograph and biography, see this issue, p. 583.

David K. Ferry (S'61–M'62–SM'72–F'86), for a photograph and biography, see this issue, p. 583.

Dieter K. Schroder (S'61–M'67–SM'78–F'96), for a photograph and biography, see p. 170 of the January 1997 issue of this TRANSACTIONS.